



Microstructural Characteristic of Dissimilar Welded Components (AISI 430 Ferritic-AISI 304 Austenitic Stainless Steels) by CO₂ Laser Beam Welding (LBW)

Uğur ÇALIGÜLÜ¹, Halil DİKBAŞ², Mustafa TAŞKIN^{1*}

¹*Firat University, Faculty of Technology, Dep. of Metallurgy and Materials Engineering, Elazığ/TURKEY*

²*Firat University, Faculty of Technical Education, Department of Metal Education, Elazığ/TURKEY*

Received: 11.01.2011 Revised: 26.03.2011 Accepted: 20.09.2011

ABSTRACT

In this study, microstructural characteristic of dissimilar welded components (AISI 430 ferritic-AISI 304 austenitic stainless steels) by CO₂ laser beam welding (LBW) was investigated. Laser beam welding experiments were carried out under argon and helium atmospheres at 2000 and 2500 W heat inputs and 100-200-300 cm/min. welding speeds. The microstructures of the welded joints and the heat affected zones (HAZ) were examined by optical microscopy, SEM, EDS and XRD analysis. The tensile strengths of the welded joints were measured. The result of this study indicated that; the width of welding zone and HAZ became much thinner depending on the increased welding speed, on the other hand, this width become wider depending on the increased heat input. Tensile strength values also confirmed this result. The best properties were observed at the specimens welded under helium atmosphere, at 2500 W heat input and at 100 cm/min welding speed.

Keywords: *Ferritic Stainless Steel (AISI 430), Austenitic Stainless Steel (AISI 304), CO₂ Laser Beam Welding, Microstructural Characteristic.*

1. INTRODUCTION

Stainless steels are iron-base alloys containing 8–25 % nickel and more chromium than the 12 % which is necessary to produce passivity but less than 30 %. The steels resist both corrosion and high temperature. Stainless steels can be divided into five types as ferritic, austenitic, martensitic, duplex and precipitation-hardening [1-2].

Ferritic stainless steels are widely used due to the fact that their corrosion resistance is higher at room temperature and they are much cheaper than the other stainless steels. Ferritic stainless steels contain 16-30 % Cr within their structures in respect of addition of the

alloy element. This type of the steel can be shaped easily and resist atmospheric corrosion well and thanks to these characteristics, it has a wide range of application in architecture, interior and exterior decoration, kitchen utensils, manufacturing of wash boilers and drying machines, food industry, automotive industry, and petrochemical and chemical industries [3-4]. Austenitic-stainless steel is preferred more than other stainless-steel types due to easiness in welding process. Then, some negative metallurgic changes are taken into consideration in welding of the steels. These are given as; delta ferrite phase, sigma phase, stress-corrosion cracking, chrome-carbide precipitate between grain boundaries at 450–850 C of Cr–Ni austenitic

*Corresponding author, e-mail: mtaskin@firat.edu.tr

steels such as 18/8 joined by fusion welding in long waiting time [5].

Stainless steels can generally be welded with all methods of fusion welding and solid state welding. Out of the fusion welding methods, electric arc welding, submerged arc welding, MIG, TIG, Plasma welding, electron beam welding, resistance welding, and laser welding etc. are widely used. In the fusion welding methods for joining the stainless steel, brittle intermetallic compounds phases are produced in the fusion zone, which reduces the strength of the welding joint. However, in the LBW joining of stainless steel, because these phases are reduced, it improves the performance of the stainless steel joint [6-10].

Laser welding, using laser beam of high energy density as a heat source, is a highly efficient and precise welding method. It has some excellences, such as high energy density, focalization, deep penetration, high efficiency and strong applicability, and it is widely applied to welding zone requiring the high precision and high quality, including aviation and space flights, automobile, microelectronics, light industry, medical treatment and nuclear industry. As laser welding is a fast but unbalanced heat-circulation process, larger temperature degrees appear around the weld, therefore the residual stress and deformation of different extent can also appear in the post welding structure. All of these phenomena become important factors, influencing the quality of welding structure and the usable capability. Understanding the heat-process of welding is crucial to analyze the mechanical welding structure and microstructure as well as controlling of welding quality [11-15].

Generally, laser beam welding includes many variables; laser power, welding speed, defocusing distance and type of shielding gas, any of which may have an important effect on heat flow and fluid flow in the weld seam. This in turn will affect the penetration depth, shape and final solidification structure of the fusion zone. Both shape and microstructure of the fusion zone will considerably influence the properties of the welding zone. Many reports [16-17-18-19] on the shape and solidification structure of the fusion zone of laser beam welds in relation to different laser parameters are available. However, the effect of all influencing factors of laser welding has not been extensively researched up to now. Many studies are required for understanding the combined effect of laser parameters on the shape and microstructure of the fusion zone. The present investigation is concerned with laser power, welding speed, defocusing distance and type of shielding gas and also their effects on the fusion zone shape and final solidification structure of some stainless steels [20-25].

Curcio et al. [26] analyzed the parameters of various materials on laser welding and reported that welding power, welding speed, shielding gas, gas nozzle and the process of focusing were amidst these parameters. Zambon et al. [27] made analyses related the microstructure and tensile stages of AISI 904L super austenitic stainless steel on CO₂ laser welding and demonstrated that in flow resistance and detach tensile a decrease was observed and depending on this decrease,

there was also an increase in hardness value because of rapid cooling of the fusion zone during welding. Bertrand et al. [28] studied the Nd YAG laser welding parameters of the stainless steel and reported that laser power and the welding speed were 600-2700 W and 3-10m/min respectively, and the flow speed of the shielding gas was similar to the surface contamination or it underwent a change depending on various surface tensions. El Batahgy [29] investigated the effects of austenitic stainless steels on surface of hardness and fusion zone of laser welding parameters and indicated that penetration increased depending on the increased welding power and welding speed, a significant difference between helium and argon shielding gases was not observed, and mechanical properties (tension, hardness, bending) and fusion zone were not affected by heat input at room temperature. Ghani et al [30] analyzed the microstructural characteristics of low carbon steels on Nd:YAG laser welding and reported that depending on the increased energy input and process speed, the hardness value of the material at welding zone also increased.

Khan et al [31] analyzed the experimental design approach to the process parameter optimization for laser welding of martensitic stainless steels in a constrained overlap configuration and reported that laser power and welding speed in the range 855–930 W and 4.50–4.65m/min, respectively, with a fiber diameter of 300 mm were identified as the optimal set of process parameters. However, the laser power and welding speed can be reduced to 800–840 W and increased to 4.75–5.37m/min, respectively, to obtain stronger and better welds. Yan et al [32] analyzed the study on microstructure and mechanical properties of 304 stainless steel joints by TIG, laser and laser-TIG hybrid welding and reported that the joint by laser welding had highest tensile strength and smallest dendrite size in all joints, while the joint by TIG welding had lowest tensile strength, biggest dendrite size. The laser welding and hybrid welding are suitable for welding 304 stainless steels owing to their high welding speed and excellent mechanical properties. Ventrella et al [33] analyzed the pulsed Nd:YAG laser seam welding of AISI 316L stainless steel thin foils and reported that pulse energy control is of considerable importance to thin foil weld quality because it can generate good mechanical properties and reduce discontinuities in weld joints. The ultimate tensile strength of the welded joints increased at first and then decreased as the pulse energy increased. The process appeared to be very sensitive to the gap between couples.

In the present paper, microstructural characteristic of dissimilar welded components (AISI 430 ferritic-AISI 304 austenitic stainless steels) by CO₂ laser beam welding (LBW) process and the effects of heat inputs and welding speeds on the joint integrity were studied.

2. MATERIALS AND METHOD

Steel plates to be joined were cut at 60x70x4 mm dimensions. 60mm width is selected to achieve the standard length of 120 mm tensile test piece. The laser welding experiments were carried out under argon and helium atmospheres with Trump LazerCell 1005 laser welding machine at 2000 and 2500 W heat inputs, 100-200-300 cm/min welding speeds. Schematic illustration of LBW was given in Figure 1 [13]. AISI 430 steels comprise approximately one half of the SAE-AISI type 400 series stainless steels. They are known with their excellent stress corrosion cracking resistance and good resistance to pitting and crevice corrosion in chlorine environments. Welding is known to reduce toughness, ductility and corrosion resistance because of the grain coarsening and carbide precipitations. The grain size

gradually increases from the edge of Heat Affected Zone (HAZ) to the fusion boundary. Welding of 400 series usually requires preheat and post-weld heat treatment to minimize stress that can lead to cracking [34]. AISI 304 steels comprise approximately one half of the SAE-AISI type 300 series stainless steels. They are known with their excellent stress corrosion cracking resistance and good resistance to pitting and crevice corrosion in chlorine environments. Austenitic-stainless steel is preferred more than other stainless-steel types due to easiness it provides during the welding process. Welding of 300 series usually requires preheat and post-weld heat treatment to minimize stress that can lead to cracking [5 and 35]. The chemical compositions, mechanical and physical properties of both steels were given in Table 1, 2 and 3 respectively.

Table 1. Chemical composition of AISI 430 ferritic and AISI 304 austenitic stainless steels.

Weight (%) Composition											
Materials	Fe	C	Si	Mn	P	S	Cr	Ni	Cu	Nb	Ti
AISI 430	Balance	0.055	0.045	0.420	0.031	0.008	17.0	-	-	-	-
AISI 304	Balance	0.08	1.00	2.00	0.045	0.03	20.0	10.0	-	-	-

Table 2. Mechanical properties of AISI 430 ferritic and AISI 304 austenitic stainless steels.

Materials	Tensile Strength (MPa)	Yield Strength 0,2% (MPa)	Elongation. (%)	Microhardness (Rockwell B')
AISI 430	517	345	25	170
AISI 304	590	295	55	130-180

Table 3. Physical properties of AISI 430 ferritic and AISI 304 austenitic stainless steels.

Materials	α 10^{-6}	λ W/m °C	Ω n Ω m	E kN/mm ²
AISI 430	13	24	600	225
AISI 304	20	15	700	200
α : Thermal Expansion Coefficient (20-800 °C)		λ : Thermal Conductive (20 °C)		
Ω : Electrical Resistance (20 °C)		E: Elastic modulus (20 °C)		

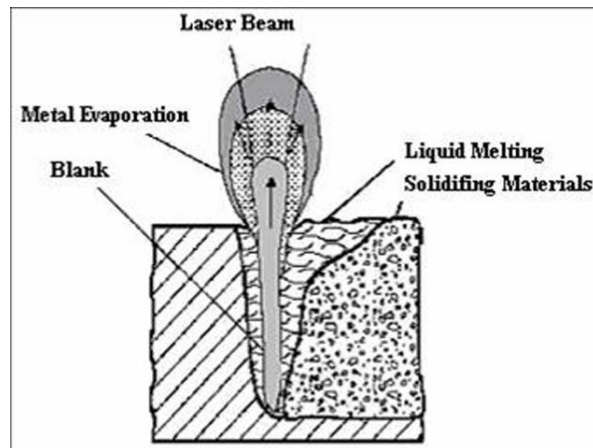


Figure 1. Schematic illustration of laser welding process.

In Figure 2 a-b-c, 3 a-b-c, 4 a-b-c and 5 a-b-c the welding samples are photographed for different heat inputs and welding speeds. The welded specimens were cut in a vertical manner to the welding zone for post evaluations of weld integrity. After the process, the samples were ground to an 80-1200-grit and they were etched by polishing them with 0.3- μm Al_2O_3 diamond paste and aqua regia, respectively. For microstructural examination, AISI 430 material was etched electrolytically in a solution of 30% HCl + 10% HNO_3 + 30 % H_2O solution and AISI 304 material was etched electrolytically in a solution of 50 % HNO_3 + 50 % H_2O solution. Then, the microstructures of the welds were studied by means of scanning electron microscopy (SEM) equipped with energy dispersive spectrometer (EDS). XRD diffraction analysis was performed to identify the structural phases. Microhardness values were measured at interface with Leica MHF-10 test apparatus and both sides were analyzed by HV scale under a load of 200 gr (Figure 6). The typical microhardness profile of the welding samples is shown in Figure 7 a-b-c-d. Then, from 120 mm length 3 pieces x 20mm (width) specimens were cut for tensile tests (Figure 8).

3. RESULTS AND DISCUSSIONS

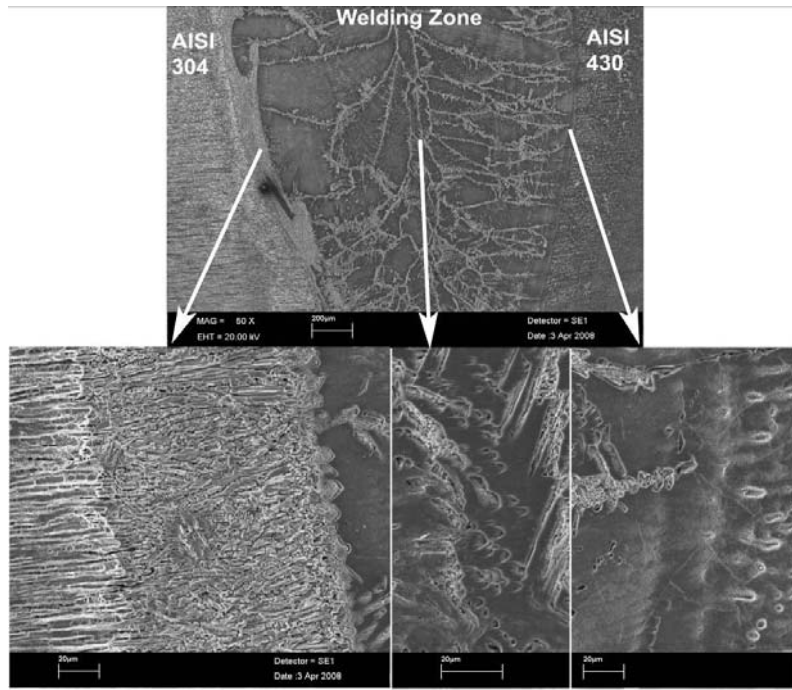
3.1. Microstructure

Welding at low travel speed (100 cm/min.) to produces more tapered weld and thus to allow more time for the escape of gases from the molten weld metal and also helps to reduce the porosity. At higher travel speeds mainly at 200 and 300 cm/min., slight incomplete penetration and missed seam were traced at weld interface.

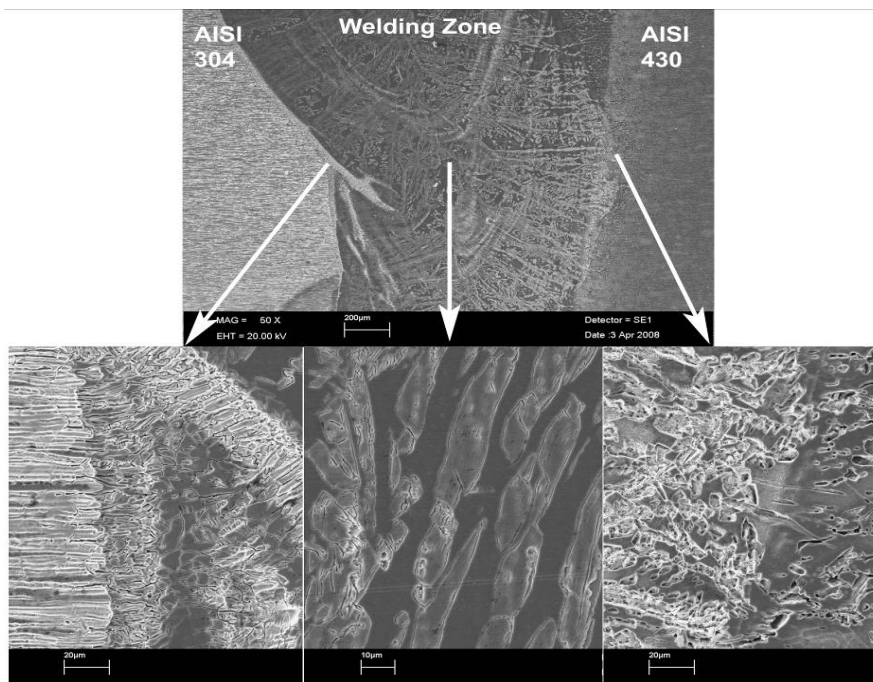
Grain coarsening was observed at HAZ at both sides of weld interface at AISI 430 ferritic and AISI 304 austenitic stainless steels side at ~ 200 - $300\mu\text{m}$ distance. Naturally, the area of weld (width) and the heat affected zone have decreased while the speeds increased because of less heat input at weld zone. Besides, the area of weld (width) can be increased depending on the increase on the heat inputs. Similar results were

achieved at the research studies by Karaaslan et al. and König et al. [34 and 36].

It was determined that at 2000 W heat input, the penetration was completed and blanks or porosities in the weld were not observed. It was seen that in joint at 100 cm/min. and under argon shielding gas, the fusion zone was $\sim 1600\mu\text{m}$ in width, whereas the fusion zone was $\sim 1150\mu\text{m}$ in width in joint at 200 cm/min. The fusion zone was $\sim 1000\mu\text{m}$ in width in joint at 300 cm/min. The deep penetration was $\sim 1550\mu\text{m}$ in depth in joint at 100 cm/min., whereas the fusion zone was $\sim 1350\mu\text{m}$ in width in joint at 200 cm/min. and the fusion zone was $\sim 1300\mu\text{m}$ in width in joint at 300 cm/min. It was seen on both sides of the welding seam that a grain hypertrophy occurred both on the AISI 430 side at $\sim 200\mu\text{m}$ distance, and on the AISI 304 side at $\sim 300\mu\text{m}$ distance. A homogeneous dispersion with small grains, beginning from the zone with coarse grains on both sides appropriate for the original structure of the materials was also observed. The hardness on the welding seam occurred vertically to the main material on the dendritic structure (Figure 2 a-b-c). In the joint of AISI 430-AISI 304 samples under helium atmosphere, the penetration was completed and blanks or porosities in the weld were not available. It was seen that in joint at 100 cm/min. and under helium shielding gas, the fusion zone was $\sim 1650\mu\text{m}$ in width, whereas the fusion zone was $\sim 1200\mu\text{m}$ in width in joint at 200 cm/min. The fusion zone was $\sim 1100\mu\text{m}$ in width in joint at 300 cm/min. The deep penetration was $\sim 1600\mu\text{m}$ in depth in joint at 100 cm/min., whereas the fusion zone was $\sim 1350\mu\text{m}$ in width in joint at 200 cm/min. and the fusion zone was $\sim 1300\mu\text{m}$ in width in joint at 300 cm/min. It was seen on both sides of the welding seam that a grain hypertrophy occurred both on the AISI 430 side at $\sim 250\mu\text{m}$ distance, and on the AISI 304 side at $\sim 300\mu\text{m}$ distance. A homogeneous dispersion with small grains beginning from the zone with coarse grains on both sides appropriate for the original structure of the materials was also observed. It was observed that the width of the welding seam and HAZ became thinner than that of the joints at 200cm/min welding speed depending on the increased welding speed (Figure 3 a-b-c).

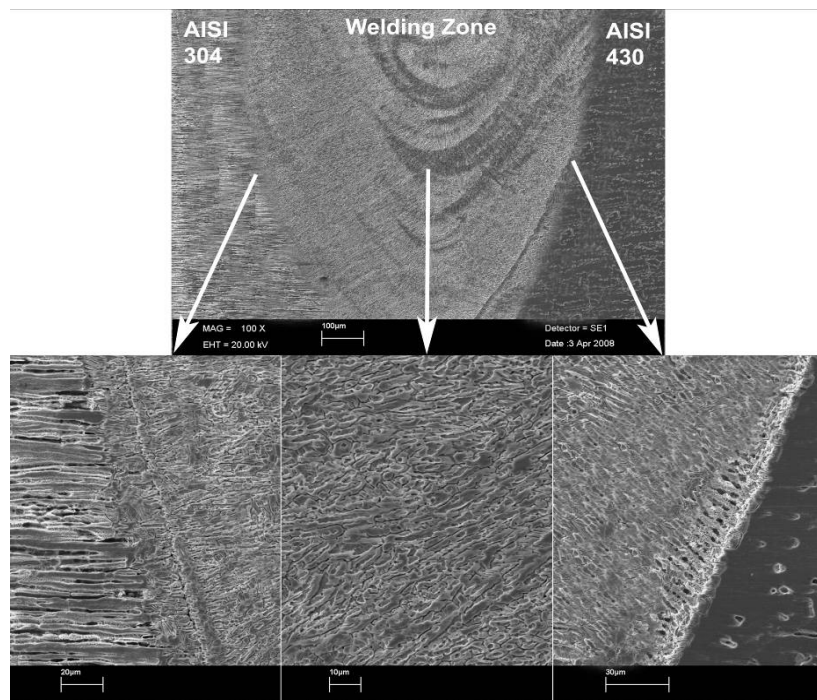


(a)



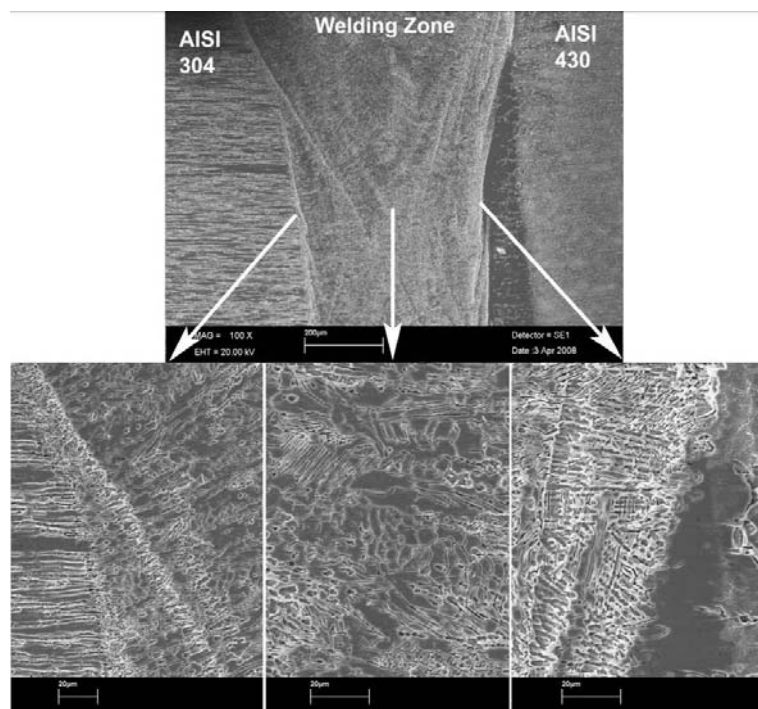
(b)

Figure 2. SEM image of welded sample joined under argon shielding gas at 2000 W heat input and at a) 100 b) 200 c) 300 cm/min. welding speeds.



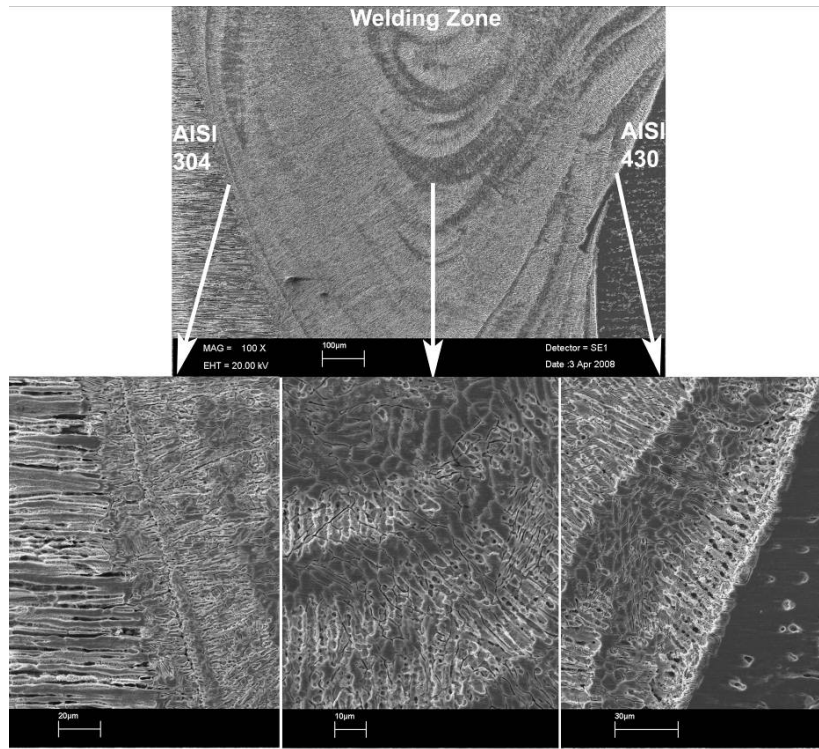
(c)

Figure 2. SEM image of welded sample joined under argon shielding gas at 2000 W heat input and at a) 100 b) 200 c) 300 cm/min. welding speeds.

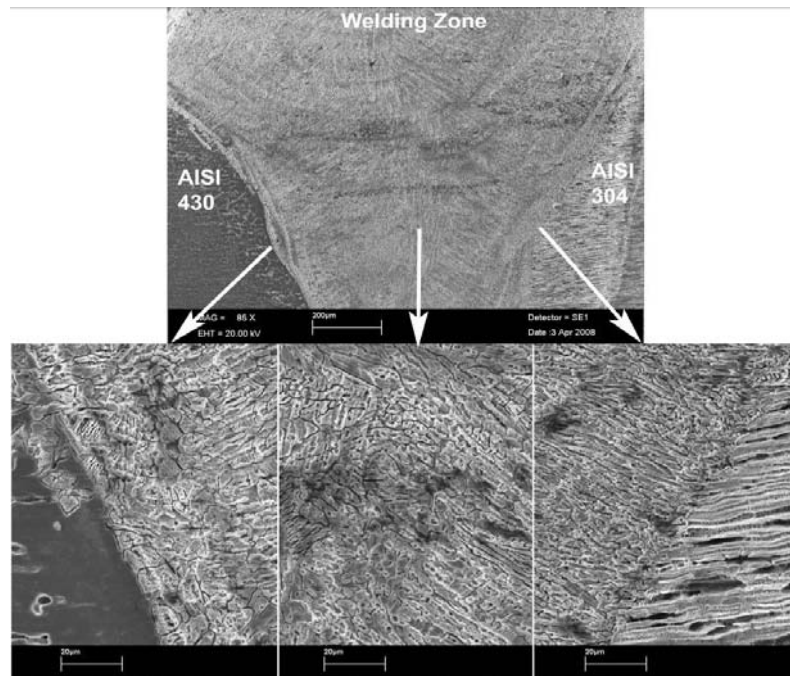


(a)

Figure 3. SEM image of welded sample joined under helium shielding gas at 2000 W heat input and at a) 100 b) 200 c) 300 cm/min. welding speeds.



(b)

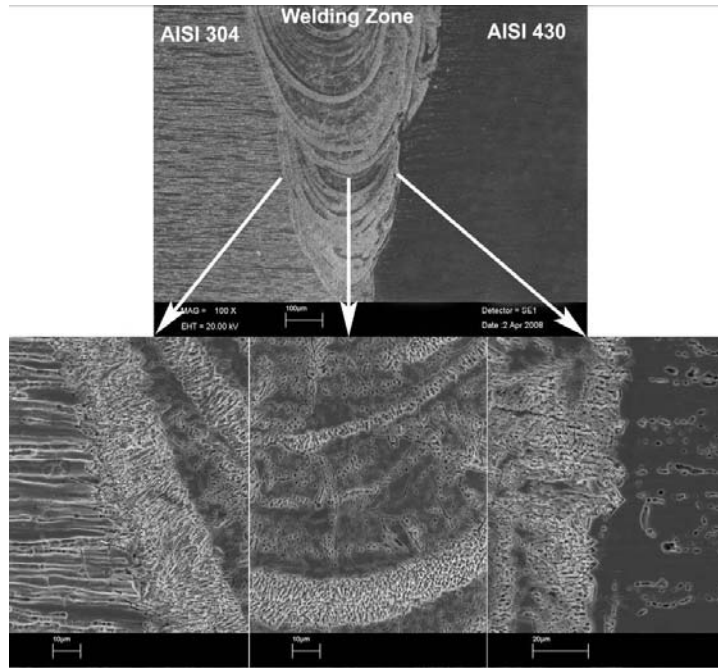


(c)

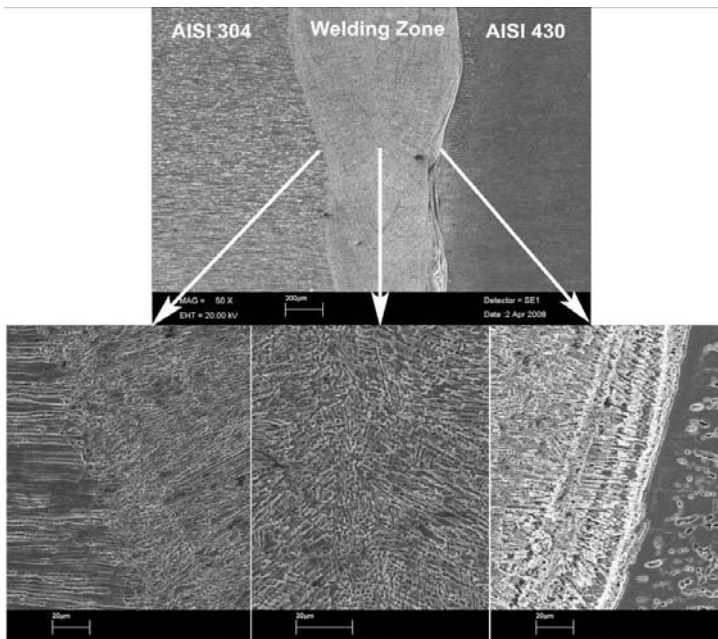
Figure 3. SEM image of welded sample joined under helium shielding gas at 2000 W heat input and at a) 100 b) 200 c) 300 cm/min. welding speeds.

It was determined that at 2500 W heat input, at 100 cm/min. and under argon shielding gas, the fusion zone was $\sim 1700\mu\text{m}$ in width, whereas the fusion zone was $\sim 1300\mu\text{m}$ in width in joint at 200 cm/min. The fusion zone was $\sim 1200\mu\text{m}$ in width in joint at 300 cm/min. The deep penetration was $\sim 1950\mu\text{m}$ in depth in joint at 100 cm/min., whereas the fusion zone was $\sim 1850\mu\text{m}$ in

width in joint at 200 cm/min. and the fusion zone was $\sim 1700\mu\text{m}$ in width in joint at 300 cm/min. It was seen on both sides of the welding seam that a grain hypertrophy occurred both on the AISI 430 side at $\sim 150\mu\text{m}$ distance, and on the AISI 304 side at $\sim 200\mu\text{m}$ distance (Figure 4 a-b-c).

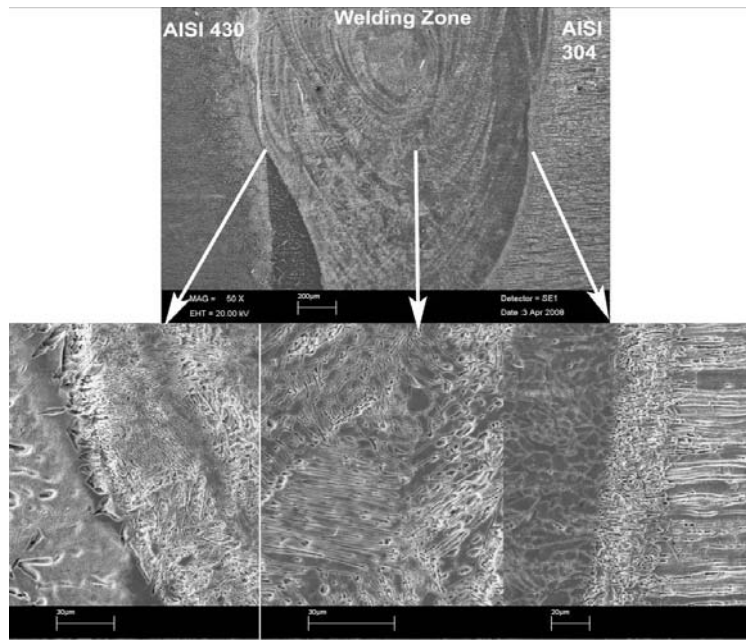


(a)



(b)

Figure 4. SEM image of welded sample joined under argon shielding gas at 2500 W heat input and at a) 100 b) 200 c) 300 cm/min. welding speeds.

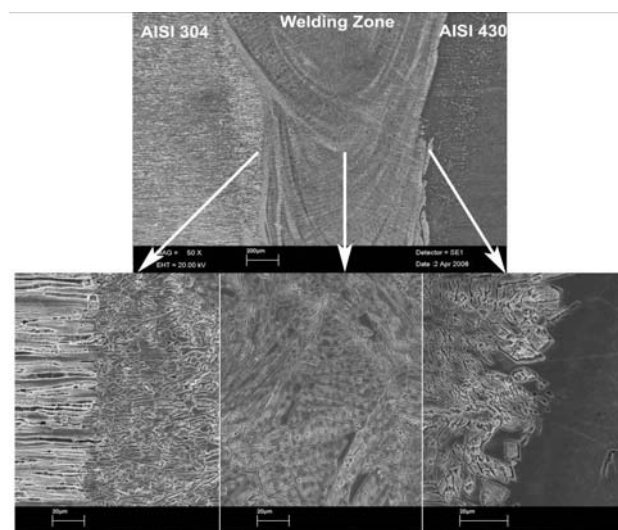


(c)

Figure 4. SEM image of welded sample joined under argon shielding gas at 2500 W heat input and at a) 100 b) 200 c) 300 cm/min. welding speeds.

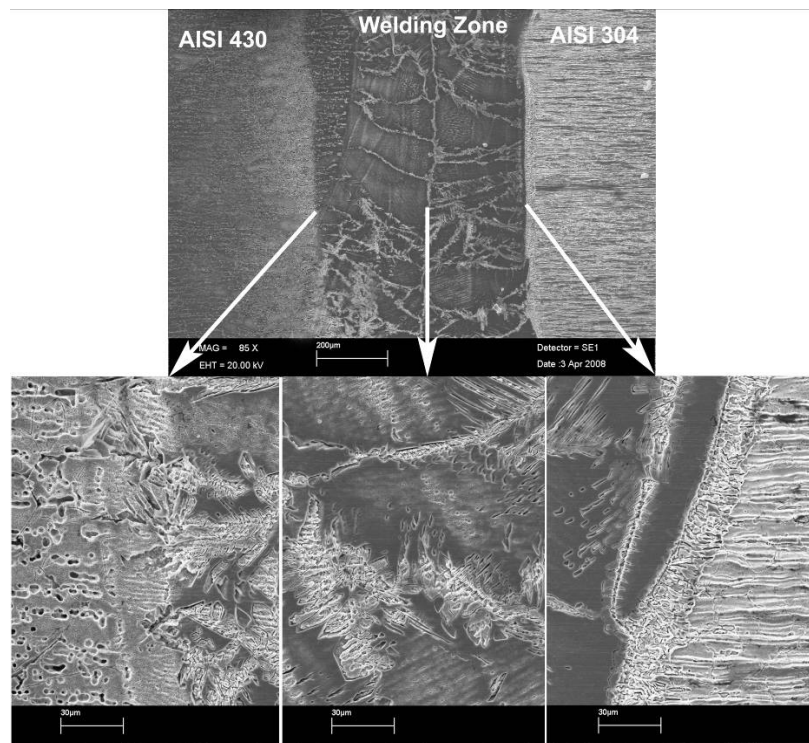
In the joint of AISI 430-AISI 304 samples with laser welding at 2500W heat input, at 100 cm/min. and under helium shielding gas, the fusion zone was $\sim 1800\mu\text{m}$ in width, whereas the fusion zone was $\sim 1400\mu\text{m}$ in width in joint at 200 cm/min. The fusion zone was $\sim 1350\mu\text{m}$ in width in joint at 300 cm/min. The deep penetration was $\sim 2000\mu\text{m}$ in depth in joint at 100 cm/min., whereas the fusion zone was $\sim 1900\mu\text{m}$ in width in joint at 200 cm/min. and the fusion zone was $\sim 1800\mu\text{m}$ in width in joint at 300 cm/min. It was seen on both sides of the

welding seam that a grain hypertrophy occurred both on the AISI 430 side at $\sim 250\mu\text{m}$ distance, and on the AISI 304 side at $\sim 350\mu\text{m}$ distance. It was determined that the grains on the welding seam first occurred vertically to the main material beginning from the first seam side where the hardness began and then the first hardened grains did not occur vertically on the dendritic structure in the inner sides of the seam (Figure 5 a-b-c).

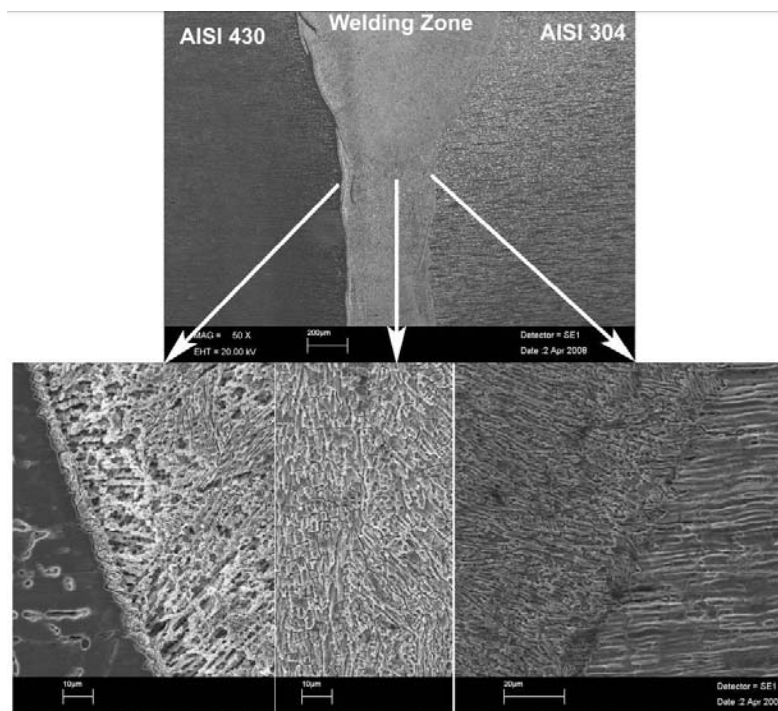


(a)

Figure 5. SEM image of welded sample joined under helium shielding gas at 2500 W heat input and at a) 100 b) 200 c) 300 cm/min. welding speeds.



(b)



(c)

Figure 5. SEM image of welded sample joined under helium shielding gas at 2500 W heat input and at a) 100 b) 200 c) 300 cm/min. welding speeds.

3.2. Microhardness

The locations of microhardness measurements and microhardness distribution of weld interface were

presented in Figure 6 and Figure 7 a-b-c-d respectively. An average value of hardness was obtained from seven measurements

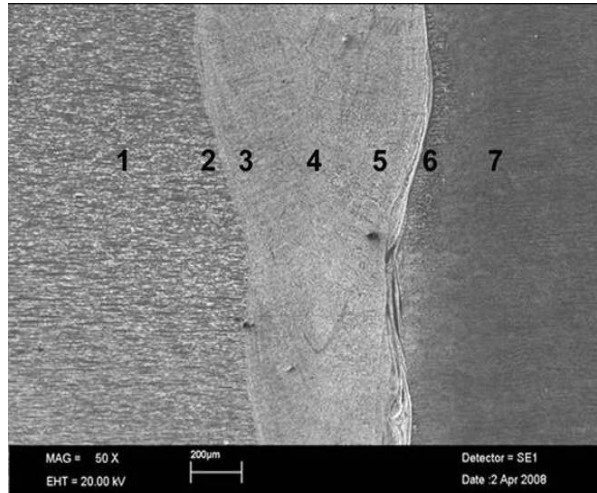


Figure 6. Locations of microhardness measurements of weld interface.

It is seen that hardness was maximum at the interface at 2000 W heat input and at 100-200-300 cm/min. welding speeds joints (about 490 HV) and decreased at different

rates toward the main material (about 210-290 HV). Microhardness values can be decreased as long as the welding speed increases.

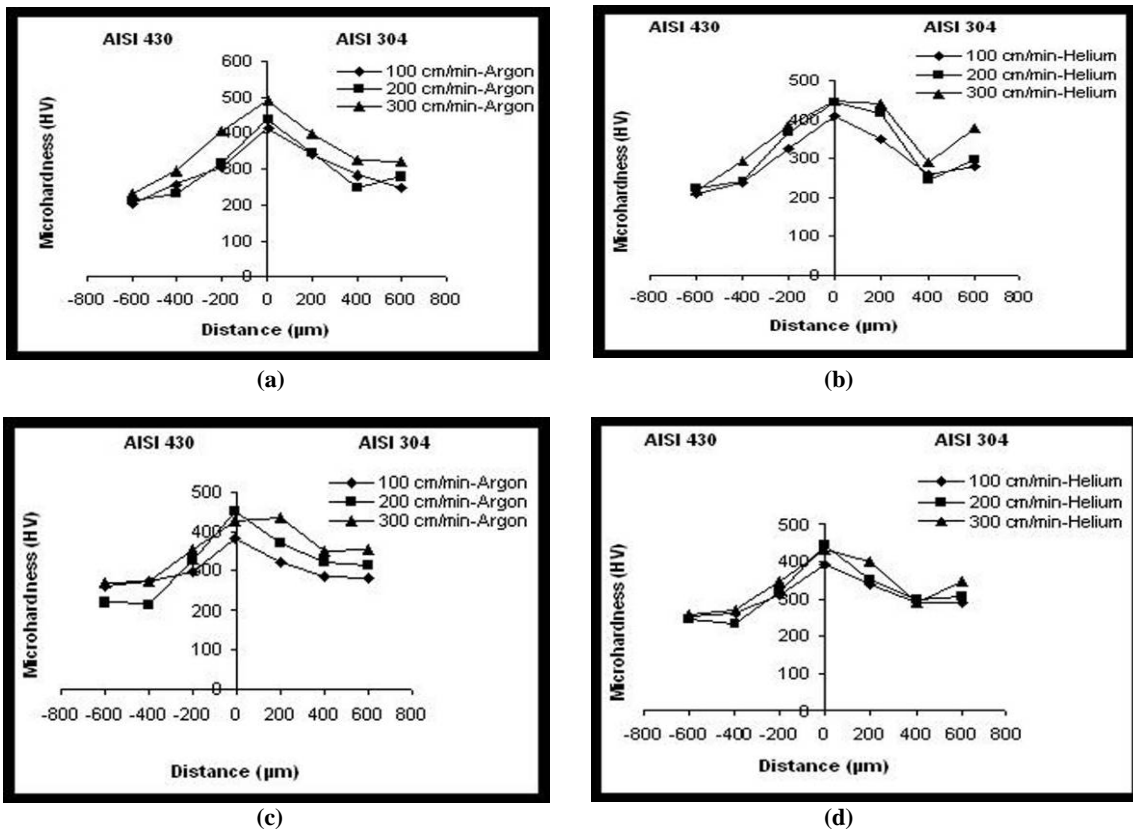


Figure 7. Microhardness values of weld interfaces a) 2000 W-Argon b) 2000 W-Helium c) 2500 W-Argon d) 2500 W-Helium

The hardness was at 2500 W heat input joints (about 550 HV) and decreased at different rates towards the main material (about 250-320 HV). This result shows similarity with Zamboni et al. and Ghaini et al. [27 and 30]. This can be explained with the Chromium, Nickel and Carbon diffusion of parent materials at weld interface, thus it has relatively lower hardness. Microhardness values of welding under argon atmosphere were lower than those of welding under helium atmosphere. This can be explained with the fact

that the specific gravity of helium is less than air, so the heat generated during welding. Depending on it, the rising of microhardness values of welding seam was obtained.

3.3. Tensile Test

After LBW, averages of 12 tensile test results on the cold tensile tests were presented in Table 4. Shape and measurements of the tensile specimens were seen in Figure 8.

Table 4. Tensile strength of welded samples joined with LBW.

Samples	Heat input (W)	Welding Speed (cm/min)	Atmosphere	Tensile Strength (MPa)
1	2000	100	Argon	373
2		100	Helium	470
3		200	Argon	339
4		200	Helium	459
5		300	Argon	236
6		300	Helium	431
7	2500	100	Argon	520
8		100	Helium	525
9		200	Argon	493
10		200	Helium	510
11		300	Argon	481
12		300	Helium	473

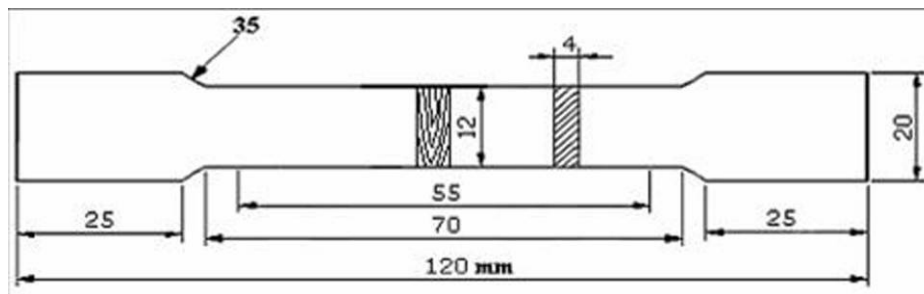


Figure 8. Shape and measurement of the tensile test specimens.

Plastic deformation detected in the specimens after the welding was not observed. This behavior can also be seen in the micrographs of the fractured surfaces (Figure 9-a-b-c-d). At tensile strength tests, fractures were observed at AISI 430 side close to interface. After welding, it is seen that tensile strength values can be decreased depending on increasing the welding speed

and this values can be increased depending on increasing the heat inputs, mainly in ductile fracture manner due to the fact that the ferritic stainless steel is a ductile steel (Figure 9-a-b-c-d). Under given conditions tensile strengths were close to parent material, and slightly decreased at increased welding speeds. This can be explained with the matter of decreased heat input.

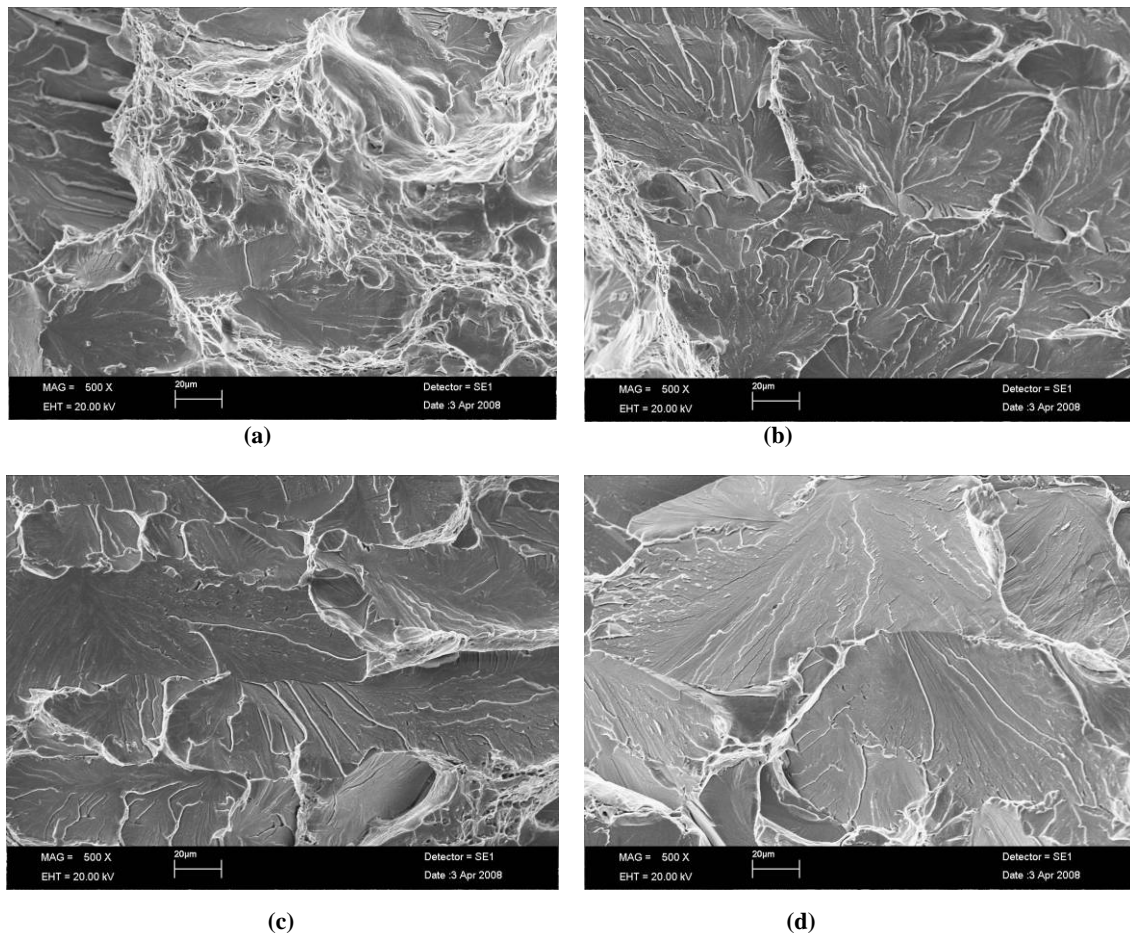


Figure 9. Micrographs of the tensile fracture surfaces of the specimens observed by SEM: a) 2000 W-100 cm/min-Argon b) 2000 W-100 cm/min-Helium, c) 2500 W-100 cm/min-Argon, d) 2500 W-100 cm/min-Helium

The lowest value according to tensile strength values, at 2000 W heat input, under argon atmosphere was obtained in the joints performed at 300 cm/min welding speed (236 MPa) and the highest value was obtained in the joints performed, at 2500 W heat input, under helium atmosphere at 100 cm/min welding speed can be seen in Table 4 (525 MPa). Tensile strength values of welding performed under argon atmosphere were lower than those of welding performed under helium atmosphere. It can be suggested that helium rises when it takes away a little heat from the atmosphere.

Therefore, better and strength welding seam was obtained.

3.4. XRD diffraction and EDS Analysis

In the EDS analysis, In the 200 µm distance, from AISI 304 austenitic stainless steel to AISI 430 ferritic stainless steel 16 % Chromium, 1,5 % Carbon and 1 % Nickel diffusion, the equal distance occurred from AISI 430 steel to AISI 304 steel Chromium and Carbon diffusion. Because, Carbon is an interstitial element and stainless steel side will diffuse more easily. It is seen that Chromium-Nickel diffusion can be decreased by increasing the welding speed (Figure 10).

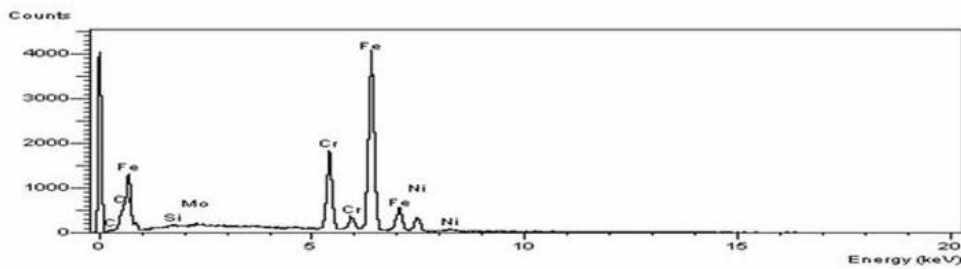
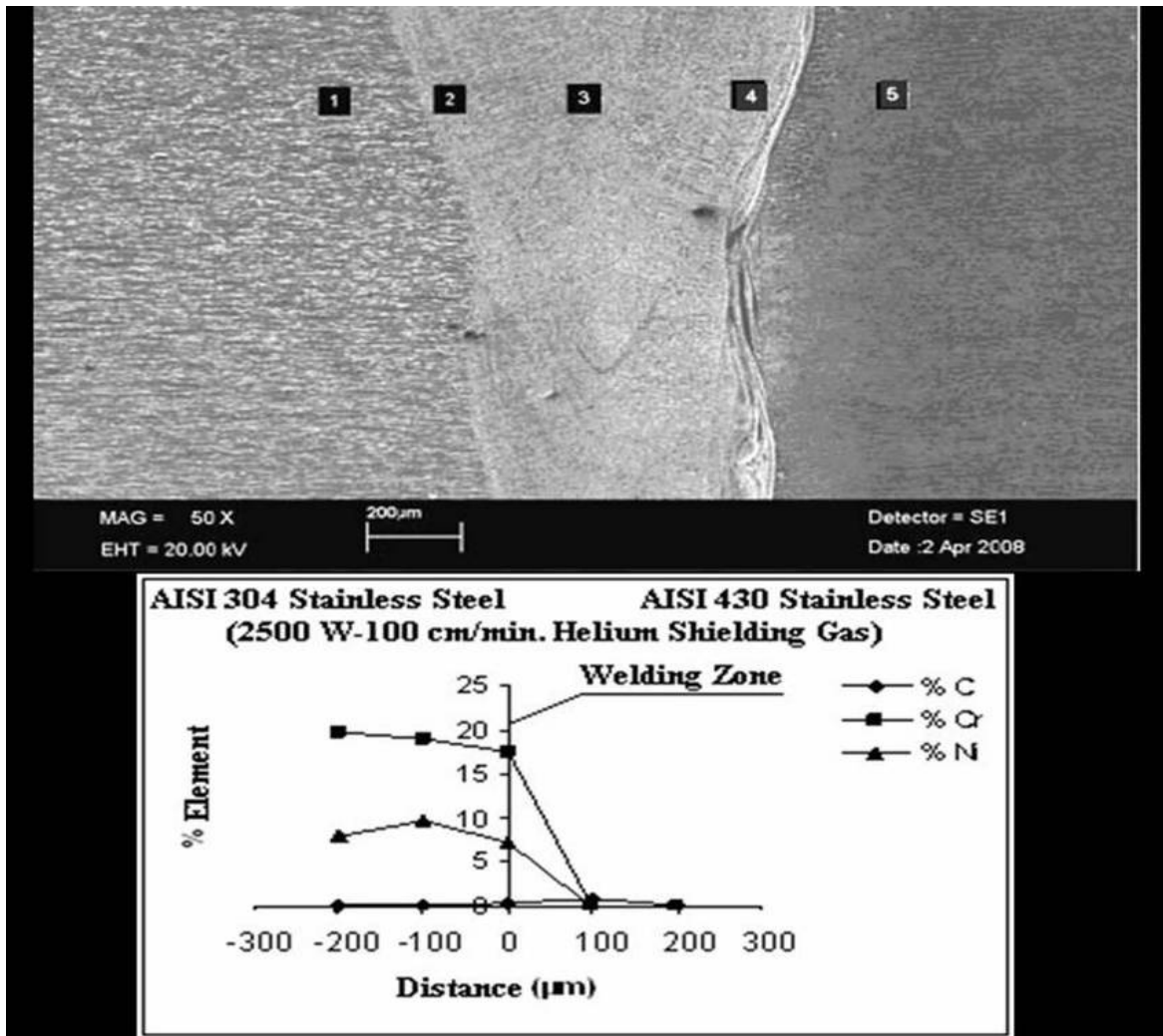


Figure 10. EDS Analysis of AISI 430/304 (2500-100-Helium) sample.

In the XRD analysis, like Fe, Ni-Cr-Fe, Fe-Cr-Co-Ni-Mo-W and $Cr_2Fe_{6.7}Mo_{0.1}Ni_{1.3}Si_{0.3}$ phases were determined (Figure 11). Intermetallic phase like $Cr_{23}C_6$

(Chromium Carbur), δ -ferrite and sigma wasn't observed.

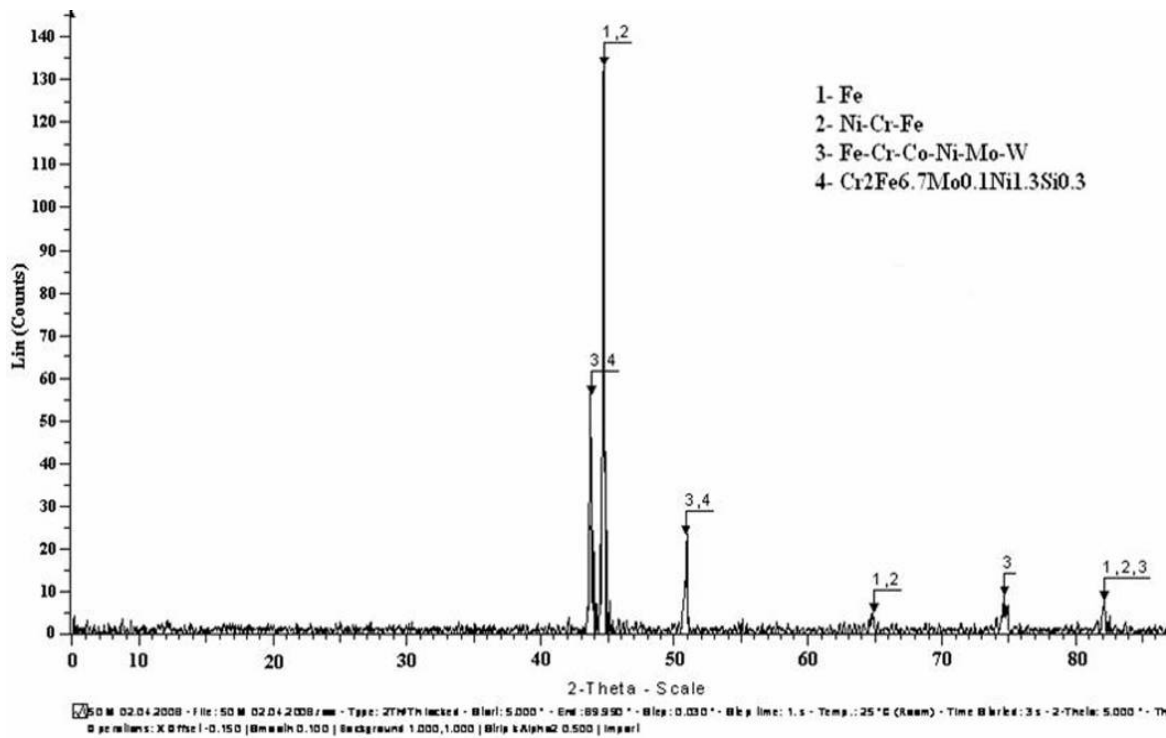


Figure 11. XRD Analysis of AISI 430/304 (2500-100-Helium) sample

4. CONCLUSIONS

In this study, microstructural characteristics of dissimilar welded components (AISI 430 ferritic-AISI 304 austenitic stainless steels) by CO₂ laser beam welding (LBW) were analyzed. The obtained results were as following:

- AISI 430 ferritic stainless steel can be joined with AISI 304 austenitic stainless steel by laser welding process using argon atmosphere, 2000 and 2500 W heat inputs, 100-200 and 300 cm/min welding speeds.
- It was seen that hardness determined maximum ~ 490 HV at the interface at 2000 W heat input and 100-200-300 cm/min. welding speeds joints and then the hardness decreased at different rates towards to the main material's hardness value (~ 210-290 HV). Microhardness values decreased due to the increasing welding speed. At 2500 W heat input the hardness was ~ 550 HV and then the hardness decreased at different rates towards to the main material's hardness value (~ 250-320 HV). Microhardness values of welding under argon atmosphere were lower than those of welding under helium atmosphere. Besides, coefficient of thermal conductivity of helium shielding gas is greater than of argon. Therefore, welding seam cools rapidly. Consequently, the microhardness values of welding seam were obtained high.
- At tensile strength tests, fractures were observed close to AISI 430 side. After welding, it was seen that tensile strength values decreased due to the increasing the welding speed. This is because of the

fact that AISI 430 is ferritic stainless steel is a ductile steel. Economically, high tensile strength with low heat input is demanded. These circumstances were obtained at 2000 W heat input, 100 cm/min. welding speed and helium shielding gas. (Table 4 (470 MPa).

- It was determined that the fusion zone was on average ~1000-1800 μm in width, the deep penetration was on average ~1300-2000 μm in depth. Coefficient of thermal expansion of austenitic stainless steel is greater than ferritic stainless steel. Therefore, on both sides of the welding seam, there was no a specific grain hypertrophy, deformation and crack formation on the main materials.
- The best properties in terms of microstructure, microhardness and tensile test were observed at the specimen bonded at 2500 W heat input, at 100 cm/min. welding speed and helium shielding gas.
- In the XRD analysis, like Fe, Ni-Cr-Fe, Fe-Cr-Co-Ni-Mo-W and Cr₂Fe_{6.7}Mo_{0.1}Ni_{1.3}Si_{0.3} phases were determined. Intermetallic phase like Cr₂₃C₆ (Chromium Carbur), δ-ferrite and sigma wasn't observed.

5. ACKNOWLEDGEMENTS

The research was supported by the Scientific and Technological Research Council of Turkey (Project No: TUBITAK -108M401).

REFERENCES

- [1] Taskin, M., Ozan, S. and Kolukisa, S., "The Effect of the Process Temperature on the Bondability in Diffusion Bonding of AISI 430 with Nodular Cast Iron", *Practical Metallography*, 43(6): 293-305 (2006).
- [2] Ozan, S., Taskin, M. and Kolukisa, S., "The Effect of the Process Temperature on the Bondability in Transient Liquid Phase (TLP) Diffusion Bonding of AISI 430 Ferritic Stainless Steel with Nodular(Spheroid) Cast Iron Using A Copper Interlayer", *Practical Metallography*, 43(11): 575-585 (2006).
- [3] Moustafa, I. M., Moustafa, M. A. and Nofal, A.A., "Carbide Formation Mechanism During Solidification and Annealing of 17% Cr-Ferritic Steel", *Materials Letters*, 42(6): 371-379 (2000).
- [4] Taskin, M. and Caligulu, U., "The Effect on the Joining of Welding Power on the Laser Welding of Couple Steels AISI 430/1010", *Firat Univ. Journal of Engineering*, 21(1): 11-22 (2009).
- [5] Sahin, M., "Evaluation of the joint interface properties of austenitic-stainless steels (AISI 304) joined by friction welding", *Materials and Design*, 28: 2244-2250 (2007).
- [6] Aran, A. and Temel, M. A., "Paslanmaz Çeliklerin Üretimi, Kullanımı, Standartları", *Sarıtaş Teknik Yayınları*, :1, 54-65 (2004).
- [7] Hussain, P. and Isnin, A., "Joining of Austenitic Stainless Steel and Ferritic Stainless Steel to Sialon", *Journal of Materials Processing Technology*, 113: 222-227 (2001).
- [8] Chih-Chun Hsieh et al., "Precipitation and Strengthening Behavior of Massive δ -Ferrite in Dissimilar Stainless Steels during Massive Phase Transformation", *Materials Science and Engineering A*, 477: 328-333 (2008).
- [9] Yilbas, B. S., Sami, M., Nickel, J., Coban, A. and Said, S.A.M., "Introduction into the Electron Beam Welding of Austenitic 321-Type Stainless Steel", *Journal of Materials Processing Technology*, 82: 13-20 (1998).
- [10] Yilbas, B. S., Shuja, S. Z., Arif, A. and Gondal, M. A., "Laser-Shock Processing of Steel", *Journal of Materials Processing Technology*, 135: 6-17, (2003).
- [11] Yilbas, B. S., "Parametric Study to Improve Laser Hole Drilling Process", *Journal of Materials Processing Technology*, 70: 264-273 (1997).
- [12] Bayraktar, E., Kaplan D. and Yilbas, B. S., "Comparative Study: Mechanical and Metallurgical Aspects of Tailored Welded Blanks (TWBs)", *Journal of Materials Processing Technology*, 204: 440-450 (2008).
- [13] Taskin, M., Caligulu, U. and Kolukisa S., "The Effect of Welding Speed on the Laser Welding of AISI 430 Ferritic Stainless–AISI 1010 Low-Carbon Steel", *Practical Metallography*, 46(11): 598-608 (2009).
- [14] Han GuoMing, Zhao Jian and Li JianQang, "Dynamic Simulation of the Temperature Field of Stainless Steel Laser Welding", *Materials and Design*, 28: 240-245 (2007).
- [15] "Welding, Brazing and Soldering", *Metals Handbook*, ASM 6: ISBN 0-87170-007 (1993).
- [16] Benyounis, K. Y., Olabi A. G. and Hashmi, M. S. J., "Optimizing the Laser-Welded Butt Joints of Medium Carbon Steel Using RSM", *Journal of Materials Processing Technology*, 164-165: 986-989 (2005).
- [17] Sahin, A. Z., Ayar, T., Yilbas, B. S., "Laser Welding of Dissimilar Metals and Efficiency Analysis", *Lasers in Engineering*, 19(3-4): 139-152 (2010).
- [18] Sahin, A. Z., Ayar, T., Yilbas, B. S., "Laser Welding: The First and Second Law Analysis", *International Journal of Exergy*, 7(5): 535-546 (2010).
- [19] Yilbas, B. S., Arif, A. F. M., Abdul Alem, B. J., "Laser Welding of Low Carbon Steel and Thermal Stress Analysis", *Optics & Laser Technology*, 42: 760–768 (2010).
- [20] Mazumder, J., "Laser Beam Welding", *ASM 6*: 262-269 (1993).
- [21] Abbott, D. H and Albright C. E., "CO₂ Shielding Gas Effects in Laser Welding Mild Steel", *Journal of Laser Applications*, 6: 69-80 (1994).
- [22] Johnson, D., Penn, W. and Bushik, S., "Application Experiences with Laser Beam Welding", *Alabama Laser*, 1-5 (2008).
- [23] Anawa E. M. and Olabi, A. G., "Control of Welding Residual Stress for Dissimilar Laser Welded Materials", *Journal of Materials Processing Technology*, 204: 22-33 (2008).
- [24] Benyounis, K. Y., Olabi, A. G. and Hashmi, M.S.J., "Effect of Laser Welding Parameters on the Heat Input and Weld-Bead Profile", *Journal of Materials Processing Technology*, 164-165: 978-985 (2005).
- [25] Alabeedi, K. F., Abboud J. H. and Benyounis, K. Y., "Microstructure and Erosion Resistance Enhancement of Nodular Cast Iron by Laser Melting", *Wear*, 266: 925-933 (2009).
- [26] Curcio et al., "On the Welding of Different Materials by Diode Laser", *Journal of Materials Processing Technology*, 175: 83-89 (2006).
- [27] Zambon, A., Ferro, P. and Bonollo, F., "Microstructural, Compositional and Residual Stress Evaluation of CO₂ Laser Welded Superaustenitic AISI 904L Stainless Steel", *Materials Science and Engineering A*, 424: 117-127 (2006).

- [28] Bertrand, P., Smurov, I. and Grevey, D., “Application of Near Infrared Pyrometry for Continuous Nd: YAG Laser Welding of Stainless Steel”, *Applied Surface Science*, 168: 182-185 (2000).
- [29] El-Batahgy A.M., “Effect of Laser Welding Parameters on Fusion Zone Shape and Solidification Structure of Austenitic Stainless Steels”, *Materials Letters*, 32: 155-163 (1997).
- [30] Ghaini et al., “Weld Metal Microstructural Characteristics in Pulsed Nd: YAG Laser Welding”, *Scripta Materialia*, 56: 955-958 (2007).
- [31] Khan, M. M. A., Romoli, L., Fiaschi, M. and Sari, F., “Experimental design approach to the process parameter optimization for laser welding of martensitic stainless steels in a constrained overlap configuration”, *Optics & Laser Technology*, 43: 158–172 (2011).
- [32] Yan, J., Gao, M., Xeng, X., “Study on microstructure and mechanical properties of 304 stainless steel joints by TIG, laser and laser-TIG hybrid welding”, *Optics and Lasers in Engineering*: 48, 512–517 (2010).
- [33] Ventrella, V. A., Berretta, J. R., Rossi, W., “Pulsed Nd:YAG laser seam welding of AISI 316L stainless steel thin foils”, *Journal of Materials Processing Technology*, 210: 1838–1843 (2010).
- [34] Karaaslan, A., Sonmez, N. and Topuz, A., “The Investigation on Non-alloyed Construction Steel Weldability with Laser”, *2. International Welding Technology Conference*, Istanbul (1998).
- [35] Sahin M. and Akata H. E., “An experimental study on friction welding of medium carbon and austenitic stainless steel components”, *Industrial Lubrication Tribology*, 56(2): 122-129 (2004).
- [36] Konig, R. and Otmanboluk, N., “Metal Cutting and Welding Process with CO₂ and Nd-YAG Laser”, *2. International Welding Technology Conference*, Istanbul (1998).